Int J Adv Manuf Technol
DOI 10.1007/s00170-013-5307-0

ORIGINAL ARTICLE

A simple approach to analyze process damping in chatter vibration

Erol Türkeş · Süleyman Neşeli

Received: 2 April 2013 / Accepted: 9 September 2013

Abstract This paper investigates how changes in chatter amplitude and frequency depend on process damping effect in dynamic turning process. For this purpose, the two degrees of freedom (TDOF) cutting system was modeled, and for an orthogonal turning system, the process damping model with a new simple approach was developed. To further explore the nature of the TDOF cutting model, a numerical simulation of the process was developed by this model. This simulation was able to overcome some of the weaknesses of the analytical model. The equations of motion for this cutting system were written as linear and nonlinear in the τ-decomposition form. The variation in the process damping ratios for different work materials was simply obtained by solving the nonlinear differential equations. A series of orthogonal chatter stability tests were performed for the identification of dynamic cutting force coefficients, using AISI-1040, Al-7075, and Al-6061 work materials, at a constant spindle speed. Finally, the experimental results were analyzed and compared with the simulation model, and it was observed that the results obtained through the experiments comply with the simulation model results.

Keywords Chatter vibration · Cutting stability · Process damping

E. Türkeş
Department of Mechanical Engineering, Dumlupinar University, Kutahya, Turkey
e-mail: eturkes@dpu.edu.tr

S. Neşeli (✉)
Department of Mechanical Technologies, Selcuk University, Konya, Turkey
e-mail: sneseli@selcuk.edu.tr

S. Neşeli
e-mail: sneselii@gmail.com

1 Introduction

Chatter is not desired, and it is formed independently from the machine tool and the outside environment. Self-excited chatter vibration occurs in metal cutting if the chip width is too large with respect to the dynamic stiffness of the system. Under such conditions, these vibrations start and quickly grow. The cutting force becomes periodically variable, reaching considerable amplitudes, and chip thickness varies in the extreme so much that it becomes dissected [1]. According to the literature [2–5], the process damping occurs due to penetration of the tool in the low cutting speeds. In the subsequent studies, the focus of the research on dynamic cutting shifted towards the identification and modeling of dynamic cutting force coefficients. The results of the CIRP effort on dynamic cutting are summarized by Tlusty [4] where the difficulty of the measurements and the inconsistency of the test data from different labs are discussed. The contact forces due to flank–wave interaction contribute to the dynamics of the cutting process by increasing the overall damping acting on the system [5–9]. Sisson and Kegg [5] concluded that the edge hone on the tool, cutting speed, and the clearance angle are the most important factors that affect process damping. In a recent study, Altintas et al. [10] developed a dynamic force model which includes chip thickness, velocity, and acceleration terms. They identified dynamic cutting force coefficients from the series of dynamic cutting tests, where the cutting tool is oscillated by a fast tool servo at the desired frequency and amplitude. The methods used in the recent studies [1, 11, 12] are based on the stability limits obtained from chatter tests and do not require as complicated measurement systems as used in many other studies. The average process damping coefficient is identified from the difference between the stability limits determined at low and high speeds, then an energy balance relation is established to relate the flank–wave contact area to

Published online: 28 September 2013

the process damping, where an indentation force coefficient is identified.

Modeling and simulation of cutting forces in machining are often required in monitoring, planning, optimization, and control of machining processes as well as in fixture design and servomechanism design. Knowledge of the cutting forces in high-speed machining is an important criterion to determine the machinability of a workpiece material. Information on cutting forces is significant because it denotes information involving the cutting process, workpiece material, cutters, fixturing elements, and machine tool itself. Thus, it provides a key basis to constitute to the basic understanding of the kinematics and dynamics of machine tools and machining processes. They can also be used to optimize cutter geometry and assess the likelihood of workpiece distortion. In particular, cutting forces have always been used as a process parameter to correlate to the significance of tool wear. Here, static force magnitude is interpreted as an average value within a specified time domain of the sampled data to establish cutting force magnitude. On the other hand, the dynamic force is associated with the oscillation between an ambient value at the beginning of a cut and reaches to a maximum at the end of the cut [13–17]. However, the magnitude of the process damping ratio (PDR) and its effects on stability has not been studied. In these studies, the modeling of the cutting system was performed due to the fact that cutting tool is constituted as a result of penetration to the rough surface of the workpiece. Penetration force and variations of cutting force that occur from penetration into a wavy workpiece surface of the tool have been studied. The variable cutting force which occurs due to variation in shear angle (φ) has also been studied. The comprehensive modeling of the dynamic cutting forces and its effects on the chatter vibration has been studied, where dynamic cutting coefficients were obtained [1, 12, 18].

In this paper, a dynamic cutting system with two degrees of freedom (TDOF) is modeled prior to the orthogonal cutting, which in general forms a mechanical cutting basis for all cutting processes. This dynamic system is used for turning. This cutting process was modeled according to τ-decomposition form, and then, the stability of this system was investigated by applying the τ-decomposition form to Nyquist criteria [1, 12, 18, 19]. Dynamic force equations of the dynamic cutting system were expressed as linear and nonlinear differential equations. The solutions of the dynamic force equations were performed by Runge–Kutta method [20]. To investigate the effect of cutting conditions on the process damping using this new method, a series of turning experiments were carried out for AISI-1040, Al-7075, and Al-6061 work materials, at a constant spindle speed and tool length. To investigate the effect of cutting conditions on the process damping,variation of the PDR for different work materials has simply been obtained by linearizing the nonlinear differential equations.

2 Modeling of the dynamic cutting system

Machine chatter prediction and stability analysis are conducted for a turning process with TDOF. Since the dynamic cutting operations are complicated, the turning system which is investigated in this study was simplified by modeling mass-spring-damper, as shown in Fig. 1.

The equations of motion of the cutting system in the feed (x) and tangential (y) directions were formed as follows:

$$\begin{aligned} m_x \ddot{x}(t) + c_x \dot{x}(t) + k_x x(t) &= F(t) \sin \beta_n \\ m_y \ddot{y}(t) + c_y \dot{y}(t) + k_y y(t) &= F(t) \cos \beta_n \end{aligned} \quad (1)$$

Where,

$$F(t) = a K_f h(t) \quad (2)$$

$$h(t) = h_0 - x(t) + x(t-\tau) \quad (3)$$

The terms in Eqs. (1–3) are as follows: a is the axial depth of cut (meter), m_x and m_y are the equivalent mass coefficients (kilogram), c_x and c_y are the structural damping coefficients (kilogram per second), k_x and k_y are the stiffness coefficients (newton per meter), k_f is the specific cutting energy of the

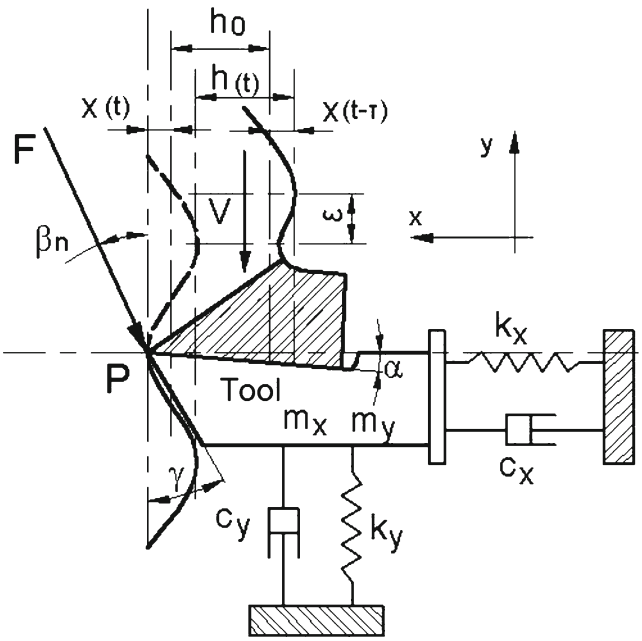

Fig. 1 Dynamic cutting model with TDOF

material (newton per square meter), $h(t)$ and h_0 are dynamic and nominal chip thicknesses (meter), respectively, and $x(t)$ and $x(t-\tau)$ are modulations of the inner and outer work surface (meter), respectively. The terms used in Fig. 1 are as follows: α is tool rake angle, β_n is the angle between dynamic resultant cutting force (F) and y axis, γ is the tool clearance angle, ε is phase delay between inner and outer modulation on the workpiece, and τ is phase delay between present time and one spindle revolution period before (second). Time delay magnitude is not constant due to the motion of cutting tool in y direction for TDOF as can be seen from Fig. 1. As it is much easier to deal with constant delay terms, the equations of motions were converted in terms of arc length "q," defined as follows:

$$q = V t + y \tag{4}$$

where V is constant linear velocity of the cutting tool relative to the workpiece (meter per second), y is displacement in y direction of the tool according to workpiece (meter), and q is the chip arc length for one period of the rotating workpiece.

3 Linear modeling of the cutting forces

One of the most important sources of instability is the so-called regenerative effect, in which cutting forces are the functions of tool–workpiece relative position at instant of machining, and phase delay (τ). The magnitude of delay is usually equal to the time of the revolution of the workpiece (or tool), in the case of a tool with single cutting edge or to a time fraction of this period for a tool with several cutting edges uniformly distributed. The problems of dynamic analysis for such systems have been thoroughly studied. At present, the dynamics of multiple cutter tools with irregularly distributed cutting edges has not yet been completely analyzed. The difficulty arises due to the presence of two or more delays, considerably complicating the problem [21]. For the TDOF model, the magnitude of the time delay τ is not constant due to (y) direction displacement. Because constant delay terms are much easier to deal with, the equations of motions are converted to a form in terms of chip arc length, q, defined as Eq. (4). When the derivative of Eq. (4) is taken as time related,

$$\frac{dq}{dt} = q_t = (V + \dot{y}) \approx V$$

Here, the displacement velocity of tool in y direction ($\dot{y}$) is neglected because it is much lesser than the linear velocity of workpiece (V). So, $\dot{x}$, $\ddot{x}$, $\dot{y}$, and $\ddot{y}$ terms in Eq. (1) could be written as follows, respectively:

$$\frac{dx}{dt} = \frac{dq}{dt}\frac{dx}{dq} = (V + \dot{y})\, x_q \Rightarrow \frac{dx}{dt} \approx V x_q$$

$$\frac{d^2x}{dt^2} = \frac{d}{dt}\left(\frac{dx}{dt}\right) = \frac{d}{dt}\left[(V + \dot{y})\, x_q\right] = (V + \dot{y})\, x_{qq}\, q_t + \ddot{y}\, x_q \Rightarrow \frac{d^2x}{dt^2} \approx V^2 x_{qq}$$

Similarly, it can also be written in y direction:

$$\frac{dy}{dt} \approx V y_q \qquad \frac{d^2y}{dt^2} \approx V^2 y_{qq}$$

If instantaneous dynamic chip thickness ($h(t)$) is expressed in the terms of chip arc length $h(q)$, then the equations of motion in (x) and (y) directions can be written as:

$$\begin{aligned} m_x V^2 x_{qq} + c_x V x_q + k_x x &= -F_x h(q) \\ m_y V^2 y_{qq} + c_y V y_q + k_y y &= -F_y h(q) \end{aligned} \tag{5}$$

Where,

$$h(q) = x(q) - x(q-\pi d) \qquad F_x = K_f a \sin\beta_n \qquad F_y = K_f a \cos\beta_n$$

Here, terms x_q and y_q indicate derivatives with respect to arc length rather than time. The delay term is now the constant length (πd) rather than the varying length of time. If both sides of Eq. (5) are reduced for simplification,

$$\widetilde{c}_x = \frac{c_x}{m_x V} \qquad \widetilde{k}_x = \frac{k_x}{m_x V^2} \qquad \widetilde{F}_x = \frac{-F_x}{m_x V^2}$$

$$\widetilde{c}_y = \frac{c_y}{m_y V} \qquad \widetilde{k}_y = \frac{k_y}{m_y V^2} \qquad \widetilde{F}_y = \frac{-F_y}{m_y V^2}$$

$$\begin{aligned} x_{qq} + \widetilde{c}_x x_q + \widetilde{k}_x x &= \widetilde{F}_x\,(x(q) - x(q-\pi d)) \\ y_{qq} + \widetilde{c}_y\, y_q + \widetilde{k}_y\, y &= \widetilde{F}_y\,(x(q) - x(q-\pi d)) \end{aligned} \tag{6}$$

Equation (6) can be written in a matrix form as follows:

$$\begin{bmatrix} 1 & 0 \\ 0 & 1 \end{bmatrix} \begin{Bmatrix} x_{qq} \\ y_{qq} \end{Bmatrix} + \begin{bmatrix} \widetilde{c}_x & 0 \\ 0 & \widetilde{c}_y \end{bmatrix} \begin{Bmatrix} x_q \\ y_q \end{Bmatrix} + \begin{bmatrix} \widetilde{k}_x & -\widetilde{F}_x 0 \\ -\widetilde{F}_y & \widetilde{k}_y \end{bmatrix} \begin{Bmatrix} x \\ y \end{Bmatrix} + \begin{bmatrix} \widetilde{F}_x & 0 \\ \widetilde{F}_y & 0 \end{bmatrix} \begin{Bmatrix} x(q-\pi d) \\ y(q-\pi d) \end{Bmatrix} = \begin{Bmatrix} 0 \\ 0 \end{Bmatrix} \tag{7}$$

Taking the Laplace transform and determinant to find the characteristic equation yields.

$$D(s) = s^4 + \left(\widetilde{c}_x + \widetilde{c}_y\right)s^3 + \left(\widetilde{k}_x - \widetilde{F}_x + \widetilde{c}_x\widetilde{c}_y + \widetilde{k}_y\right)s + \left(\left(\widetilde{k}_x - \widetilde{F}_x\right)\widetilde{c}_y + \widetilde{c}_x\widetilde{k}_y\right)s + \left(\widetilde{k}_x - \widetilde{F}_x\right)\widetilde{k}_y + \left(s^2 + \widetilde{c}_y s + \widetilde{k}_y\right)\widetilde{F}_x e^{-d\pi s} = 0 \tag{8}$$

To investigate the stability of the system, the characteristic equation can be arranged as follows:

$$a_4 = 1/\widetilde{F}_x \quad a_3 = \left(\widetilde{c}_x + \widetilde{c}_y\right)\Big/\widetilde{F}_x$$

$$a_2 = \left(\left(\widetilde{k}_x - \widetilde{F}_x\right) + \widetilde{c}_x\widetilde{c}_y + \widetilde{k}_y\right)\Big/\widetilde{F}_x \quad a_1 = \left(\left(\widetilde{k}_x - \widetilde{F}_x\right)\widetilde{c}_y + \widetilde{c}_x\widetilde{k}_y\right)\Big/\widetilde{F}_x$$

$$a_0 = \left(\left(\widetilde{k}_x - \widetilde{F}_x\right)\widetilde{k}_y\right)\Big/\widetilde{F}_x$$

$$D(s)/\widetilde{F}_x = a_4 s^4 + a_3 s^3 + a_2 s^2 + a_1 s + a_0 + \left(s^2 + \widetilde{c}_y s + \widetilde{k}_y\right)e^{-d\pi s} = 0 \tag{9}$$

Putting $D(s)$ equal to 0, this becomes:

$$e^{d\pi s} = \frac{-\left(s^2 + \widetilde{c}_y s + \widetilde{k}_y\right)}{a_4 s^4 + a_3 s^3 + a_2 s^2 + a_1 s + a_0} \tag{10}$$

If Eq. (10) is separated into two parts, it can be written in the form below:

$$U_1(s) = e^{d\pi s} \quad U_2(s) = \frac{-\left(s^2 + \widetilde{c}_y s + \widetilde{k}_y\right)}{a_4 s^4 + a_3 s^3 + a_2 s^2 + a_1 s + a_0}$$

According to the Nyquist criteria, the right side of this equation expresses Nyquist plane curve $U_2(s)$, while the left side expresses the critical orbit $U_1(s)$. If $s = j\omega$, then the roots of the characteristic Eq. (10) can be obtained by equalizing the magnitude of the right side of Eq. (1):

$$\frac{\left|\left(\widetilde{k}_y - \omega^2\right) + j\widetilde{c}_y\omega\right|}{\left|\left(a_4\omega^4 - a_2\omega^2 + a_0\right) + j\left(a_1\omega - a_3\omega^3\right)\right|} = 1$$

$$\left(a_4\omega^4 - a_2\omega^2 + a_0\right)^2 + \left(a_1\omega - a_3\omega^3\right)^2 = \left(\widetilde{k}_y - \omega^2\right)^2 + \widetilde{c}_y{}^2\omega^2$$

The characteristic equation yields:

$$a_4^2\omega^8 + \left(a_3^2 - 2a_4a_2\right)\omega^6 + \left(a_2^2 + 2a_4a_0 - 2a_3a_1 - 1\right)\omega^4 + \left(a_1^2 - \widetilde{c}_y{}^2 - 2a_2a_0 + 2\widetilde{k}_y\right)\omega^2 + a_0^2 - \widetilde{k}_y^2 = 0 \tag{11}$$

Hence, the positive real root of this equation gives the chatter frequency of the system.

4 Nonlinear modeling of the cutting forces (process damping)

When long shafts are turned in manufacturing, the machine tool is often configured such that the workpiece does not rotate, but is fed at an axial velocity, V, to rotating cutters. It is observed that such a configuration yields a more accurately machined workpiece surface due to decreased lateral shaft vibrations. The variation in the cutting force is caused by the variation in the effective chip thickness or the rate of penetration of the tool. As a consequence, the cutting force depends upon the actual and delayed values of the relative displacement of the tool and the workpiece, where the length of the delay is equal to the time period of the revolution of the workpiece. Only the change in the cutting force needs to be considered since the constant force can be eliminated by the proper choice of the coordinate origin. To this end, consider the delay differential equation for a dynamic cutting model [22]. To further explore the nature of the TDOF cutting model, a numerical simulation of the process was developed. The simulation is able to predict the time domain response of the system described by Eqs. (1), (2), and (3) without the need for the simplifications and modifications introduced to obtain an analytical solution. This is the system demonstrated in Fig. 1. In this regard, if $\dot{y}$ is not neglected in Eq. (4), Eq. (5) can be written as follows:

$$\begin{aligned} m_x\left[x_{qq}q_t^2 + \ddot{y}\,x_q\right] + c_x x_q q_t + k_x x &= -F_x h(q) \\ m_y\left[y_{qq}q_t^2 + \ddot{y}\,y_q\right] + c_y y_q q_t + k_y y &= -F_y h(q) \end{aligned} \tag{12}$$

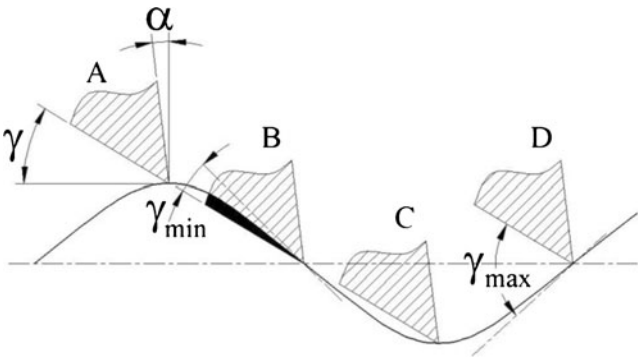

Fig. 2 Penetration model of cutting tool

Similarly, both sides of Eq. (12) are reduced for simplification:

$$\widetilde{c}_{1x} = \frac{c_x}{m_x q_t} \qquad \widetilde{k}_{1x} = \frac{k_x}{m_x q_t^2} \qquad \widetilde{F}_{1x} = \frac{-F_x}{m_x q_t^2}$$

$$\widetilde{c}_{1y} = \frac{c_y}{m_y q_t} \qquad \widetilde{k}_{1y} = \frac{k_y}{m_y q_t^2} \qquad \widetilde{F}_{1y} = \frac{-F_y}{m_y q_t^2}$$

and by taking into account $\mu = \frac{\ddot{y}}{q_t^2}$, Eq. (6) can be written as:

$$x_{qq} + \left(\mu + \widetilde{c}_{1x}\right) x_q + \widetilde{k}_{1x}\, x = \widetilde{F}_{1x}\,(x(q) - x(q - \pi d)) \qquad (13)$$

$$y_{qq} + \left(\mu + \widetilde{c}_{1y}\right) y_q + \widetilde{k}_{1y}\, y = \widetilde{F}_{1y}\,(x(q) - x(q - \pi d))$$

Hence, Eq. (13) can be written in matrix form as:

$$\begin{bmatrix} 1 & 0 \\ 0 & 1 \end{bmatrix} \begin{Bmatrix} x_{qq} \\ y_{qq} \end{Bmatrix} + \begin{bmatrix} \mu + \widetilde{c}_{1x} & 0 \\ 0 & \mu + \widetilde{c}_{1y} \end{bmatrix} \begin{Bmatrix} x_q \\ y_q \end{Bmatrix} + \begin{bmatrix} \widetilde{k}_{1x} & -\widetilde{F}_{1x} 0 \\ -\widetilde{F}_{1y} \widetilde{k}_{1y} & \end{bmatrix} \begin{Bmatrix} x \\ y \end{Bmatrix} + \begin{bmatrix} \widetilde{F}_{1x} & 0 \\ \widetilde{F}_{1y} & 0 \end{bmatrix} \begin{Bmatrix} x(q - \pi d) \\ y(q - \pi d) \end{Bmatrix} = \begin{Bmatrix} 0 \\ 0 \end{Bmatrix} \qquad (14)$$

The characteristic equation of the TDOF system can be written the same as Eq. (8). Total damping coefficients (c_x and c_y) of the cutting system in the x and y directions are increased by μ as shown in Eq. (13). Also, μ was obtained by penetration of the tool into the wavy workpiece surface as shown in Fig. 2.

Penetration of the tool occurs during semi-period of the tool oscillation as shown in Fig. 2, where μ is process damping coefficient of the cutting system. Calculation of the μ is performed numerically. In this study, an adaptive Runge–Kutta method was used for numerical integration scheme. Runge–Kutta methods compute the state of a system, in this case the velocity and displacement of the cutting tool, at a series of discrete time steps. The numerical program computes the next state using a fourth-order integration technique. As can be seen from Fig. 2, the cutting tool position from A to C is a half of the vibration period of the tool. Penetration of the cutting tool into the workpiece wave surface is from A to B and the γ angle decreases, than cutting tool exit from immersion between the positions of B and C, and the γ angle increases up to the D position [2]. According to these explanations, the value of c_x and c_y increases from A to B and decreases symmetrically from B to C. Thus, the investigation of tool motion only from A to B is enough. As seen in Fig. 2, penetration of the cutting tool into the workpiece wave surface is maximum and cutting tool moves downward in y direction. Thus, linear cutting speed V_c of the tool in this region will be in minimum values.

$$V_c = q_t = V - \dot{y} \qquad (15)$$

When the tool is on the location B, the linear cutting speed will be as below:

$$V_c \cong q_t \cong V \qquad (16)$$

For a stable cutting, $\frac{d^2y}{dt^2} = q_t^2 y_{qq} + \ddot{y}\, y_q = 0$.

Where,

$y_q = \frac{dy}{dq}$ and $y_{qq} = \frac{d^2y}{dq^2} = \frac{d(dy)}{dq^2} = \frac{d}{dq}\,\frac{dy}{dq}$

$$\dot{y} = \frac{dy}{dt} = \omega_c dr \quad \Rightarrow \quad dr = \frac{dy}{dt}\,\frac{1}{\omega_c}$$

$$q_t = \frac{dq}{dt} = \frac{d(2\pi r)}{dt} = 2\pi \frac{dr}{dt} = \frac{2\pi}{\omega_c}\,\frac{dy}{dt}$$

Finally, the acceleration equation above can be written as:

$$q_t^2 \frac{d}{dq}\,\frac{dy}{dq} + \ddot{y}\frac{dy}{dq} = 0$$

Table 1 Test device properties

Device	Range	Sensitivity	Power	Other
Impact hammer	0–500 N	10 mV/N	20–30±5 V	27.0 kHz
Accelerometer	−5…. +5 g	104.3 mV/g	5 V	40.0 kHz
NI-DAQ card	16 input/2 output	500 kS/s	5 V	12 bit
Microphone	40–18,000 Hz		11–52 V	

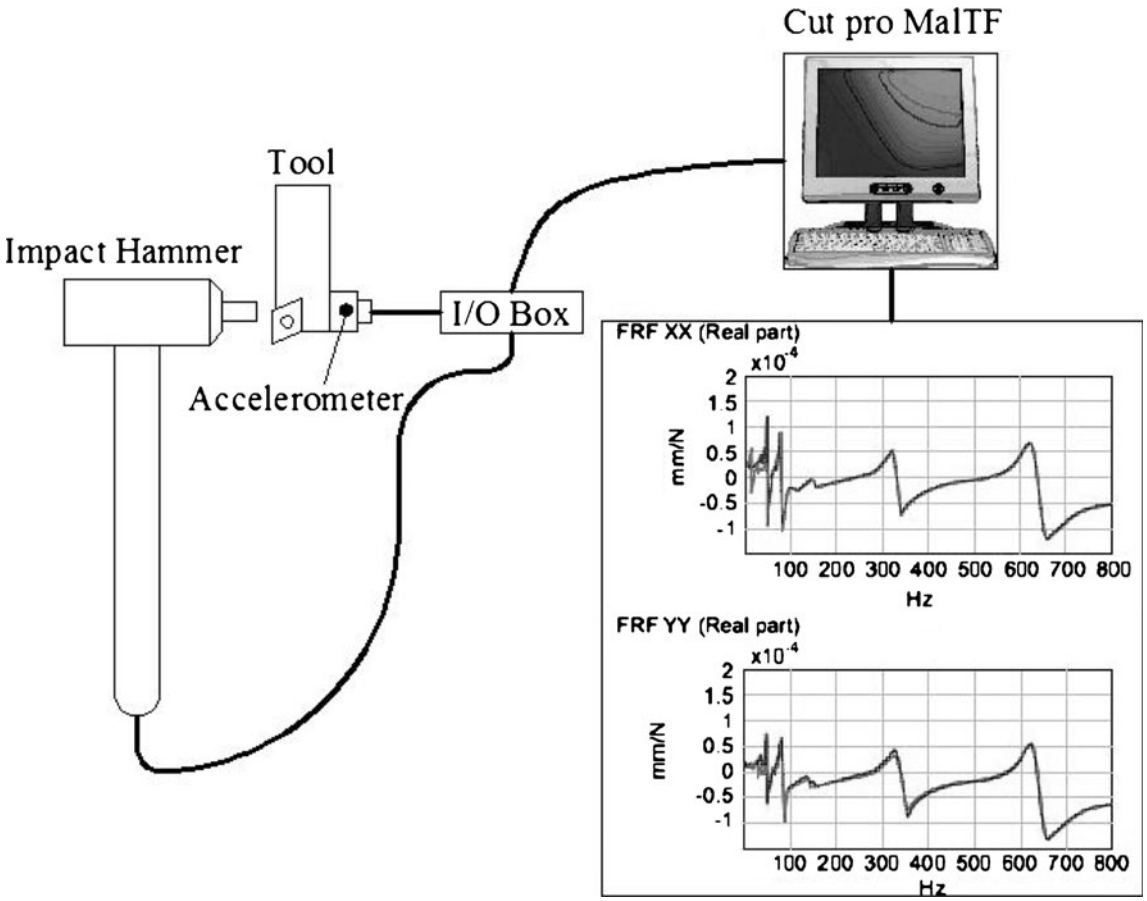

Fig. 3 Experimental setup for impact hammer test

After solving both sides of the above equation:

$$q_t \frac{d}{dt} + \ddot{y} = q_t f_c + \ddot{y} = 2\pi f_c \frac{dr}{dt} + \ddot{y} = 0$$

Hence,

$$f_c^2 \dot{y} + \ddot{y} = 0 \tag{17}$$

For numerical solution of linear differential equation, the boundary conditions are $0 \le t \le T_c$ and the starting conditions for B location were $y(0)=A_y$ and $\frac{dy}{dt}(0) = 0$. where A_y, T_c, and f_c are chatter amplitude, period, and chatter frequency (hertz) in the y direction of the tool, respectively.

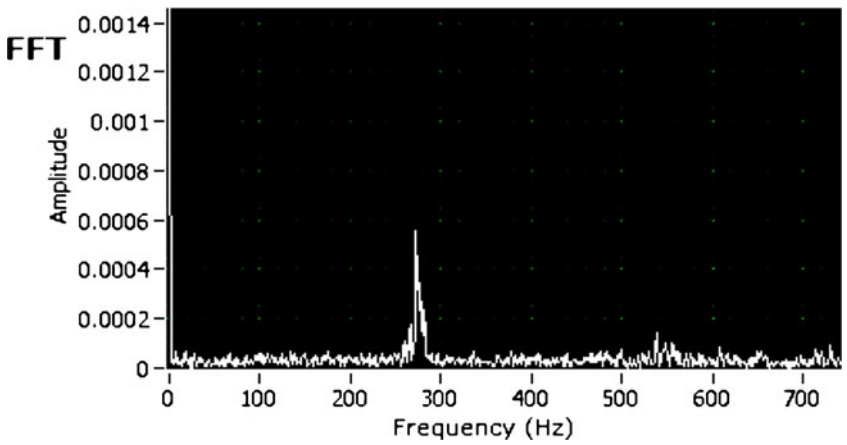

Fig. 4 Sample result of microphone test

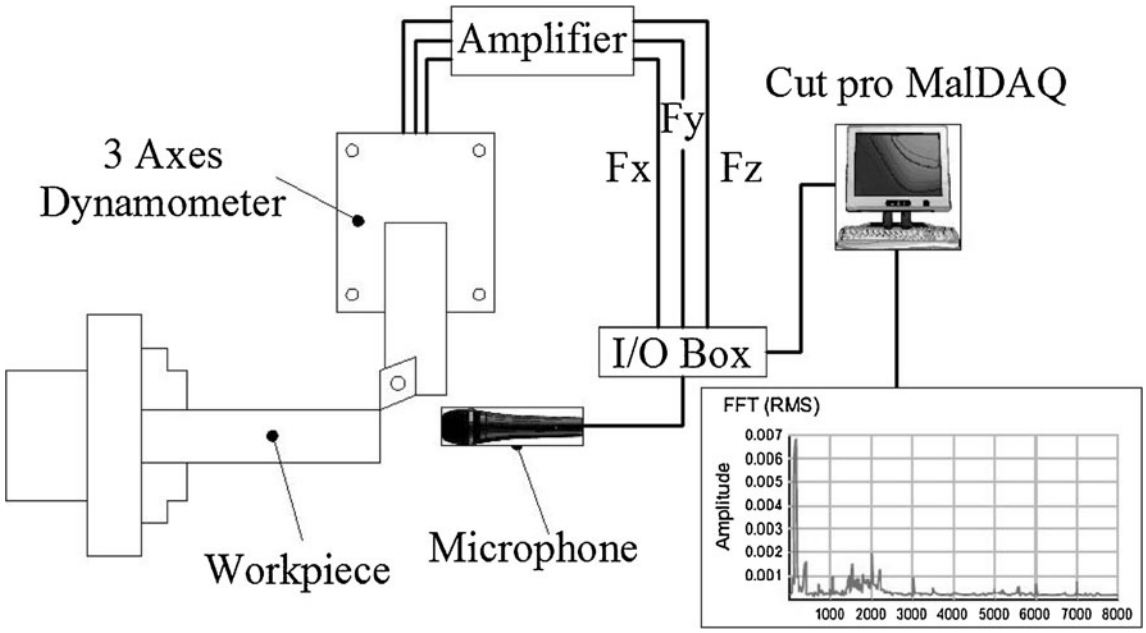

Fig. 5 Experimental setup for microphone test

5 Stability analysis

To understand the chatter phenomenon completely, we must resort to the nonlinear aspects as it has been shown that chatter is an essentially nonlinear phenomenon. According to the nonlinear theory of chatter, some typical chatter phenomena, such as finite amplitude chatter and bifurcations, can explain which the linear theory cannot explain. According to the linear theory of chatter, there are distinct stability boundaries in the process parameter space. The stability behavior undergoes an abrupt change from stable to unstable, which is not the real case for the nonlinear situation [22]. There have been many theoretical investigations regarding stable and unstable operating ranges for various cutting conditions. These works

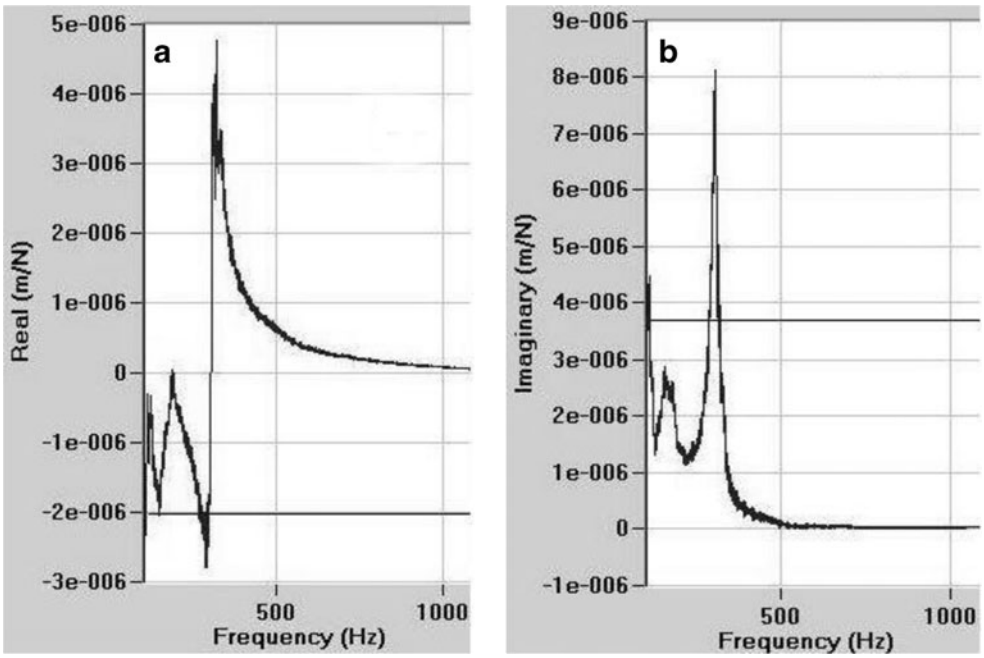

Fig. 6 **a** Real and **b** imaginer graphics obtained from modal analysis of the TDOF system

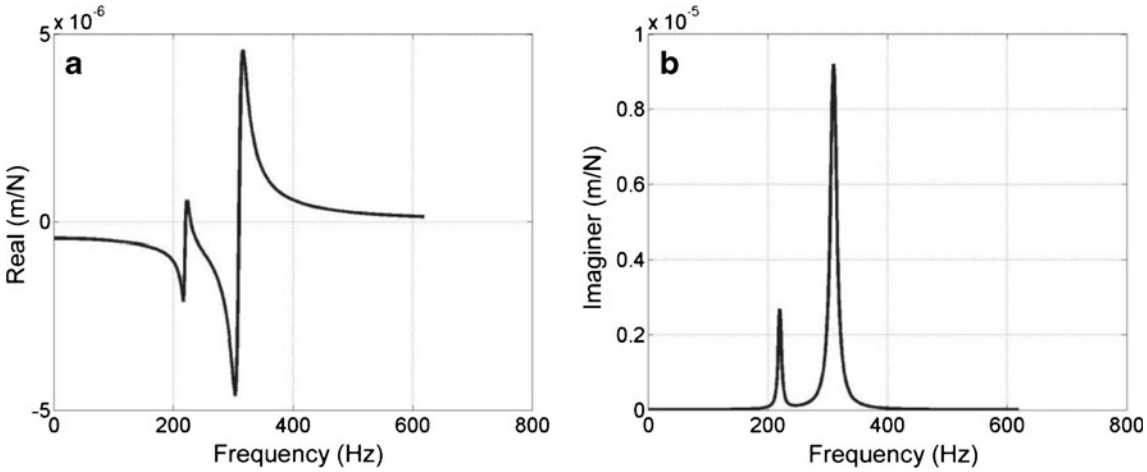

Fig. 7 Transfer function of a TDOF system represented by its (**a**) real and (**b**) imaginary parts

typically rely on constructing models and varying one parameter (cutting speed, width of cut, etc.) at a time in order to generate stability lobe diagrams showing regions of stable and unstable cutting. The simplest models model the tool as a single degree of freedom under damped linear oscillator excited by the variation in undeformed chip thickness from one revolution to another. More complicated models introduce nonlinear damping and stiffness in order to explain the bounded nature of the oscillations in chatter. However, it has been shown that the nonlinear relationship between the cutting force and the uncut chip thickness has a stronger effect on the global dynamics than the nonlinearity of the structural stiffness and damping. Experimental efforts in chatter often are conducted to validate the aforementioned analytically derived stability limits. There are also cases where data-driven techniques are used to predict the onset of chatter or active control is used to eliminate it. The simplest approaches to chatter detection rely on heuristically determining a magnitude threshold value (usually in the frequency domain). This is a logical approach since the most obvious manifestation of chatter is larger amplitude dynamics. This has been done with measuring tool displacement, force, acceleration, or acoustic emission. More robust chatter detection algorithms look at the organization or entropy of cutting signals as opposed to the magnitude because it has been noted that chatter results in a transition from more stochastic higher dimension dynamics to more deterministic lower dimension dynamics [23, 24].

In this study, we considered the orthogonal cutting which is probably the most chatter-prone cutting mechanism there is. Hence, the roots of Eq. (11) must now be obtained for stability analysis of the cutting system. The number of roots found will be twice the number that is actually present in the system. As a result, only the positive real roots of the equation need to be examined. Each positive real root (ω_i) is substituted back into the equation $U_2(s)$ to find $U_2(j\omega_i)$. Hence, Nyquist curve is drawn. The curve of Eq. $U_1(s)$ is a critical orbital curve (unit circle). According to the Nyquist criteria, the right side of Eq. (11) expresses Nyquist curve $U_2(s)$ and the left

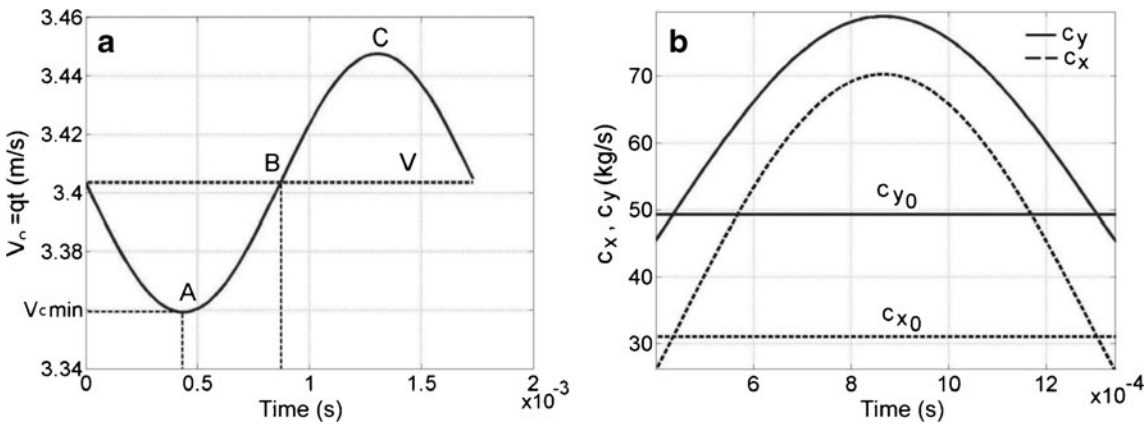

Fig. 8 The variation of **a** cutting speed and **b** damping constants

Table 2 Orthogonal cutting parameters for work materials

Material	f_c (Hz)	A (μm)	ζ (%)	a_{lim} (mm)	K_f (N/m^2)x10^9
AISI-1040	289	8.5	0.025	1.5	1.67
Al-7075	263	2.9	0.013	3.5	0.7
Al-6061	297	2.5	0.011	4.3	0.72

f_c chatter frequency, A amplitude, ζ process damping ratio, a_{lim} stable axial cutting depth, K_f cutting force coefficient

side expresses critical orbit $U_1(s)$. With the help of the real and imaginer parts of the equation $U_2(j\omega_i)$, the phase angle is found.

$$\psi_i = \tan^{-1}\frac{Im(U_2(j\omega_i))}{Re(U_2(j\omega_i))} \tag{18}$$

Delay value is found as in the following:

$$\tau_i = \frac{\psi_i + 2\pi k}{\omega_i} k = 0, 1, 2, \ 3 \tag{19}$$

Similarly, the ratio of imaginer (H) to real (G) parts of the characteristic function, these parts obtained from oriented transfer function of turning system with the TDOF, gives phase shift of the structure's transfer function.

$$\psi = \tan^{-1}\frac{H}{G} \tag{20}$$

The corresponding spindle period and maximum spindle speed are found as:

$$\tau = \frac{\varepsilon + 2\pi k}{\omega_c} k = 0, 1, 2, 3 \tag{21}$$

$$N = {}^{60}/_{\tau} \tag{22}$$

where ω_c is chatter frequency of cutting tool (radian per second); k is number of full waves formed on the cutting surface; and ε is phase shift between the inner and outer waves, calculated as $\varepsilon = 3\pi + 2\psi$. The corresponding critical axial depth of cut for each spindle speed

$$a_{\text{lim}} = \frac{-1}{2K_f G(\omega)} \tag{23}$$

is calculated [1].

6 Empirical study and numerical simulations

In the current study, AISI-1040, Al-7075, and Al-6061 materials have been used as a workpiece material whose diameters are 65 mm. As a cutting condition of the turning process, the spindle speed (N) is 1,000 rpm, feed rate (h_0) is 0.12 mm/rev, and the rake angle (α) is 6°. The workpiece is cut by Kennametal (SDJR-2525M11 NA3) inserts on universal lathe TOS SN50C. Tool holder dimensions are 25×25×135 mm ($b \times h \times l$) and tool length is L=70 mm. According to these data, the cutting force angle (β_n) was calculated from orthogonal mechanics (Turkes et al. 2011a) as 20°. Modal analysis of the turning system was performed by the impact hammer test. Some important properties of hammer test devices and experimental setup were given in Table 1 and Fig. 3, respectively.

After that, the modal parameters were determined by using CutPro_MalTF software and CutPro_Modal software. According to these analyses, the damping ratios, stiffness coefficients, and natural frequencies in x and y directions, respectively, are obtained as ζ_x=1.34 %, ζ_y=2.00 %, k_x= 1.6×10^6 N/m, k_y=2.4×10^6 N/m, f_{nx}=200 Hz, and f_{ny}= 310 Hz. These results were obtained during the cutting operation under the cutting conditions, which were mentioned above, by using a microphone connected to PC and processed by LabVIEW 7 software that is loaded into the same computer. The chatter frequencies in dynamic cutting are obtained by microphone tests (see Fig. 4). Test device properties used in

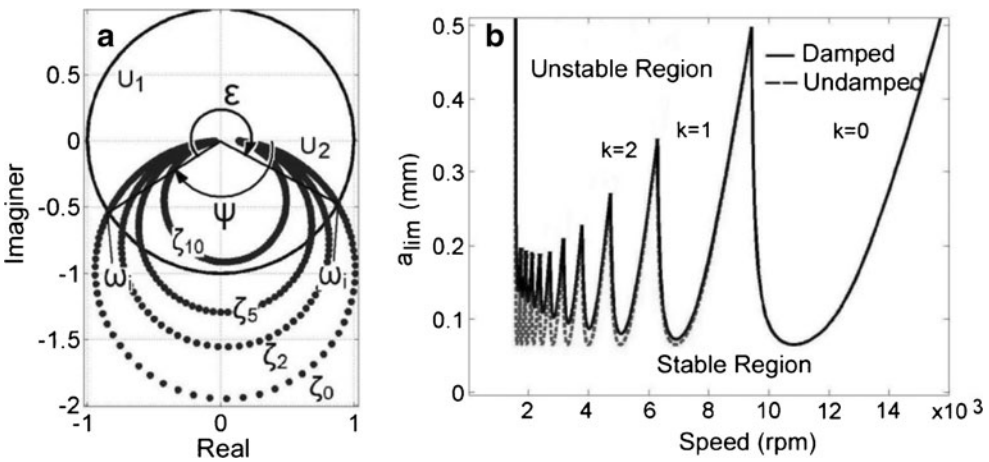

Fig. 9 The variation of **a** Nyquist and **b** stability lobe diagram

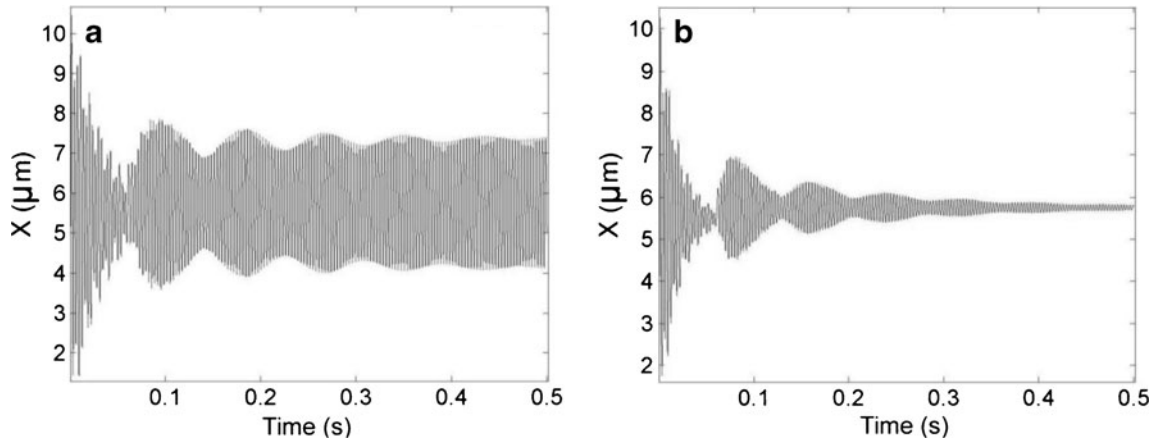

Fig. 10 The tool displacement. **a** Undamped. **b** Damped

the cutting tests and dynamic cutting test setup are given as Table 1 and Fig. 5, respectively.

Real and imaginer graphics of the TDOF turning system which were obtained from the modal analysis test for exemplarily AISI-1040 have been shown in Fig. 6a, b. Also, the real and imaginer parts of the simulated transfer function of the cutting system for comparison with experimental results are given in Fig. 7a, b. Thus, the frequency corresponding to the minimum negative real part of the transfer function can be predicted as chatter frequency. This value, according to the form calculated here, was predicted to be 289 Hz. Prediction chatter frequency in both calculation forms is explained in this study, and as expected, it is greater than the natural frequency that was found as a result of the modal analysis of the system.

As mentioned earlier, due to the tool vibration in the x and y directions, the tool displaced during the cutting. As seen in Eq. (13), the damping constants of the system with TDOF change according to tool position in the y direction which varies in accordance with $\dot{y}$ and $\ddot{y}$. In addition, due to $\dot{y}$ between the tool and workpiece, the relative cutting speed V_c was varied. Thus, the variations of c_x and c_y have been found by linearized solving of the nonlinear equations of $\dot{y}$ and $\ddot{y}$ during cutting in a tool period which vibration amplitude and frequency of tool were measured, where the variation of V_c during a vibration period has been shown in Fig. 8a. According to Fig. 2, when tool is on the point A, V_c receives the minimum value; when the tool tip is on the point B, it becomes $V_c = V$; and when the tool is on the point C, V_c receives the maximum value. The chatter frequency, amplitude, process damping ratio, maximum stable axial depth, and specific cutting energy values of the material for AISI-1040, Al-7075, and Al-6061 were given in Table 2. Also, process damping values for different spindle speed range and work materials were given by Neşeli [18].

According to Fig. 1, point B is on the nominal depth of cut axis which is initially equal to tool feed rate. As mentioned earlier, c_x and c_y increase between A and B points and symmetrically reduce between B and C points. c_x and c_y variations between these points have been shown in Fig. 8.

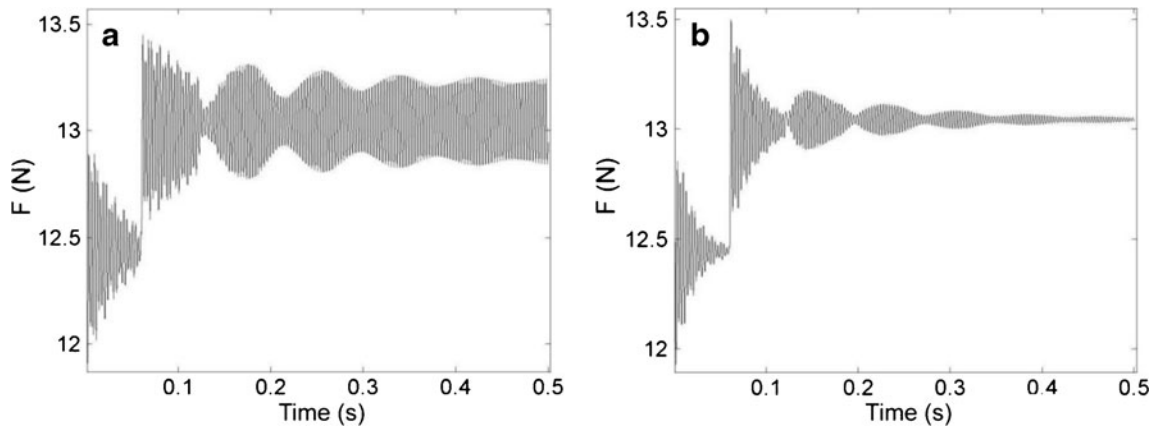

Fig. 11 The variation of cutting force. **a** Undamped. **b** Damped

For a linearized numerical solution of Eq. (13) determined as $0 \le t \le_{Tc}$ for Eq. (23) as a boundary condition, distances were divided into 200 equal parts. As shown in Fig. 8a, b, for c_x and c_y variation, consideration between A and B range will be enough. This range is divided into ten equal parts and the corresponding c_x and c_y values substituted in the modeling procedure described above, $U_1(\omega_i)$ Nyquist unit circle, and $U_2(\omega_i)$ Nyquist place curve were plotted as can be seen in Fig. 9a. Here, the damping constants ($\varsigma_{x,y} = c_{x,y}/2\sqrt{k_{x,y}\, m_{x,y}}$) expressed in terms of damping ratio, the situations of 0, 2, 5, and 10, respectively, are plotted as $U_2(\omega_i)$ curves. Using procedure between Eqs. (18) and (23), the stability lobe diagram was plotted in Fig. 9b for TDOF turning system. Undamped stability lobe diagram is shown with a dashed line, which is observed from the linear modeling. A continuously drawn thicker line is obtained according to variation range of the ς_x and ς_y, which is obtained from the solution of the linearized nonlinear model. Here, a higher stability is observed in the low cutting speed.

In this study, time domain simulation of TDOF system has been performed; therefore, how the changes affect tool displacement or chatter amplitude, X (micrometer), and resultant cutting force, F (newton), from damping ratio are examined. In the simulation, the one step time is selected as 1×10^{-4} and the total time step quantity is divided into 5,000 equal pieces and the period of workpiece is divided into 200 equal pieces. The limit axial depth of cut ($a_{\lim}$) was calculated by Eq. (23). According to these data, the tool displacements plotted with damped and undamped were shown in Fig. 10a, b. Figure 10a represents a clearly unstable case, where the amplitude of the vibrations is much larger. Figure 10b shows the simulated amplitude of vibrations with the effect of process damping. It can be seen that process damping in turning has a more significant effect.

The variation of the resultant cutting force can also be seen in Fig. 11a, b. For damped and undamped situations, in these figures, the values of c_x and c_y are status values on the ς_0 and ς_{10}.

7 Conclusion

The present contribution aims to shed light on the phenomenon of process damping when machine turning. This will be achieved using a novel solution methodology, which has been presented, that relies on a frequency domain solution. The motion equations of the cutting forces in the x and y for this turning system have been written as linear and nonlinear. The relevant nonlinearity is considered only on the cutting force variation in motion of the tool in the y direction and the spring nonlinearity is not considered. For this purpose, firstly, the motion equation of the system was discussed in the τ-decomposition form. Considering the motion of the tool in the y direction during cutting, the motion equations are arranged, and thus, the characteristic equation of the system is obtained. Accordingly, the damping constants change depending on $\dot{y}$ and $\ddot{y}$ in the x and y directions. Variation of the PDR for the different work materials has been simply obtained by linearized numeric solution of the nonlinear differential equations. If the variation of c_x and c_y values substitutes into the characteristic equation, how process damping changes according to Nyquist criteria were shown within Nyquist curves and stability lobe diagrams. Lastly, process damping variation was solved by time domain simulation and its effect upon tool displacement or chatter amplitude, X (micrometer), and the resultant cutting force, F (newton), was investigated. In the present study, finally, with the modeling, a new simple approach is tried to research on the effects of process damping and how it varies. This approach allows a new interpretation on the stabilization mechanisms behind the model and is more amenable to solution when using experimentally obtained frequency response measurements of the structure.

References

1. Turkes E, Orak S, Neseli S, Yaldiz S (2011) A new process damping model for chatter vibration. Measurement 44(8):1342–1348
2. Altintas Y, Weck M (2004) Chatter stability in metal cutting and grinding. CIRP Ann Manuf Technol 53(2):619–642
3. Das MK, Tobias SA (1967) The relation between the static and the dynamic cutting of metals. Int J Mach Tool Des Res 7(2):63–89
4. Tlusty J (1978) Analysis of the state of research in cutting dynamics. CIRP Ann Manuf Technol 27(2):583–589
5. Sisson TR, Kegg RL (1969) An explanation of low-speed chatter effects. J Eng Ind 91(4):951–959
6. Wu DW (1984) A new approach of formulating the transfer function for dynamic cutting processes. J Eng Ind 111:37–47
7. Elbestawi MA, Ismail F, Du R, Ullagaddi BC (1994) Modeling machining dynamics including damping in the tool-workpiece interface. J Eng Ind 116(4):435–439
8. Lee BY, Tarng YS, Ma SC (1995) Modeling of the process damping force in chatter vibration. Int J Mach Tool Manuf 35(7):951–962
9. Shawky AM, Elbestawi MA (1997) An enhanced dynamic model in turning including the effect of ploughing forces. J Manuf Sci Eng 119(1):11–20
10. Altintas Y, Eynian M, Onozuka H (2008) Identification of dynamic cutting force coefficients and chatter stability with process damping. CIRP Ann Manuf Technol 57(1):371–374
11. Budak E, Tunc LT (2009) A new method for identification and modeling of process damping in machining. J Manuf Sci Eng(131/051019)
12. Turkes E, Orak S, Neseli S, Yaldiz S (2012) Decomposition of process damping ratios and verification of process damping model for chatter vibration. Measurement 45(6):1380–1386
13. Toh CK (2004) Static and dynamic cutting force analysis when high speed rough milling. Mater Des 25(1):41–50
14. Pratt JR, Nayfeh AH (1999) Design and modeling for chatter control. Nonlinear Dyn 19(1):49–69
15. Nayfeh AH, Nayfeh NA (2011) Analysis of the cutting tool on a lathe. Nonlinear Dyn 63(3):395–416

16. Litak G, Schubert S, Radons G (2012) Nonlinear dynamics of a regenerative cutting process. Nonlinear Dyn 69(3):1255–1262
17. Kim P, Seok J (2012) Bifurcation analyses on the chatter vibrations of a turning process with state-dependent delay. Nonlinear Dyn 69(3): 891–912
18. Neşeli S (2013) Analytical investigation of effect of process damping on chatter vibrations and optimization cutting parameters depending on stable depth of cut and process damping values in turning. Natural and Applied Science of Selcuk University, PhD thesis, Turkey
19. Turkes E, Orak S, Neseli S, Yaldiz S (2011) Linear analysis of chatter vibration and stability for orthogonal cutting in turning. Int J Refract Met Hard Mater 29(2):163–169
20. Orak S, Turkes E (2005) Investigation of cutting process damping in the chatter for turning. 1st International Vocational and Technical Education Technologies Congress, Marmara University, Technical Educational Faculty, İstanbul/Turkey 1094–1104
21. Gouskov AM, Voronov SA, Paris H, Batzer SA (2002) Nonlinear dynamics of a machining system with two interdependent delays. Commun Nonlinear Sci Numer Simul 7(4):207–221
22. Deshpande N, Fofana MS (2001) Nonlinear regenerative chatter in turning. Robot Comput Integr Manuf 17(1–2):107–112
23. Cardi AA, Firpi HA, Bement MT, Liang SY (2008) Workpiece dynamic analysis and prediction during chatter of turning process. Mech Syst Signal Process 22(6):1481–1494
24. Christopher MT, Sam T, Neil DS (2010) Chatter, process damping, and chip segmentation in turning: a signal processing approach. J Sound Vib 329:4922–4935